Mechanics of Materials 164 (2022) 104116

Contents lists available at ScienceDirect

Mechanics of Materials

journal homepage: www.elsevier.com/locate/mechmat

Predicting high cycle fatigue life with unified mechanics theory

Hsiao Wei Lee, Cemal Basaran *

Department of Civil, Structural and Environmental Engineering, University at Buffalo, USA

ARTICLE INFO

Keywords:
Entropy
Unified mechanics theory
Microplasticity
Thermodynamics
Metal fatigue
Void evolution
Failure
Fracture

ABSTRACT

Fatigue life prediction of metals has been widely studied. However, most of the research is based on empirical models under the framework of Newtonian mechanics, that relies on experimental fatigue data for curve fitting a degradation evolution function. Unified mechanics theory (UMT), on the other hand, unifies the universal laws of motion of Newton by incorporating the second law of thermodynamics directly into the Newton's laws at the ab-initio level. UMT introduces an additional linearly independent axis called Thermodynamic State Index (TSI), which can have values between zero and one. Evolution along the TSI axis follows the Boltzmann's entropy formulation and the thermodynamic fundamental equation of the material. As a result, governing differential equations of any system automatically include energy dissipation, and degradation evolution. The fatigue model presented here is pure physics based and does not require an empirical evolution function obtained by curve fitting to fatigue test data. However, it does require deriving analytical thermodynamic fundamental equations of the material based on the principals of physics. Thermodynamic fundamental equation for high cycle metal fatigue is derived in this study.

1. Introduction

A model based on the unified mechanics theory is introduced to predict high cycle fatigue life of metals. Fatigue life prediction with the unified mechanics theory eliminates the need for curve fitting an empirical evolution function to a fatigue test data. The simulation results are compared with test data. In unified mechanics theory, the degradation evolution is calculated along the thermodynamic state index (TSI) axis which is quantified by the thermodynamic fundamental equation of the material (Basaran, 2021). The coordinate values of TSI start at zero and end at one. Thermodynamic fundamental equation provides the entropy generation quantity in the material under a given load. Based on this entropy value a new coordinate is calculated according to normalized form of Boltzmann's entropy formulation of the second law. (Basaran, 2021; Boltzmann, 1877).

There are six mechanisms that generate entropy during high cycle metal fatigue. These are: configurational entropy, ΔS_c , vibrational entropy, ΔS_{vib} (Kelly et al., 2012; Abbaschian and Reed-Hill, 2009; Fultz, 2010), the entropy generation due to vacancy concentration gradient driven diffusion, ΔS_d (Basaran and Lin, 2008; Li et al., 2009), the entropy from heat conduction, ΔS_T (Basaran, 2021), the entropy generation due to atomic-friction-generated heat, ΔS_r (Basaran, 2021), and finally the entropy generation due to micro-plasticity (Lemaitre et al., 1999; Doudard et al., 2005; Charkaluk and Constantinescu, 2009; Fan et al., 2018) $\Delta S_{\mu p}$. Because entropy is an additive property, we can write the thermodynamic fundamental equation for the total entropy production as follows,

$$\Delta S = \Delta S_c + \Delta S_{vib} + \Delta S_d + \Delta S_T + \Delta S_r + \Delta S_{\mu p} \tag{1}$$

Since microplasticity is one the most important entropy generation mechanism in the current study, in the following we introduce some of the recent published research works about microplasticity theory.

(Mozafari et al., 2020) developed a thermodynamically-consistent rate-independent small strain based plastic constitutive theory to capture the inelastic microplastic work dissipation. In their paper, they derived the non-negative rate of dissipation and the kinematic relation for plastic strain rate based on the complementary energy density and the second law of thermodynamics. A dimensionless function that incorporate the smooth transition from microplastic to macroplastic flow response is introduced and implemented to the flow rule and constitutive equation. For the fatigue life prediction, they use the fatigue fracture entropy (FFE) as the threshold to estimate the number of cycle to failure. The finite element simulation shows that their model can predict the fatigue life of P355NL1 material under different variable stress amplitude strain-controlled loading blocks (Ustrzycka et al., 2020). analyzed the fatigue crack initiation in cyclic microplasticity

* Corresponding author.
E-mail address: cjb@buffalo.edu (C. Basaran).

https://doi.org/10.1016/j.mechmat.2021.104116
Received 19 April 2021; Received in revised form 30 August 2021; Accepted 19 October 2021
Available online 23 October 2021

regime. They assumed the action of local stress leads to the proceeding of damage growth, and the fluctuations of local stress are resulting from material inhomogeneities such as inclusions, grain boundaries, boundary asperities, cavities, etc. They proposed a damage growth model based on the critical plane concept model that account for local stress fluctuations, which are usually neglected in formulation of the damage models. A critical value of damage accumulation leads to the initiation of macrocracks (Teng et al., 2020a, 2020b, 2020c). proposed a unified fatigue life calculation based on intrinsic thermal dissipation and microplasticity evolution. They used the heat diffusion equation to correlated the temperature measurement to intrinsic dissipation of the material within a unit time under high cycle fatigue. The microplastic strain amplitude is obtained based on the law of localization and homogenization, and a unified energy approach. Jirandehi and Khonsari (2021) developed a statistical method to estimate the plastic strain energy during metal fatigue. In their study, the term microplasticity refers to the plastic behavior at micro-elements when nominal stress amplitude exceeds the microelement's yield limit. They used a probability function to describe the microplastic behavior when the applied cyclic load is given. The strain in the micro-element [local strain] is calculated based on a Weibull distribution. By incorporating another probability function for meeting the von-mises criterion(a grain slips on at least five independent slip systems to deform and preserve shape continuity of the material's crystal structure), the microplastic strain energy in each micro-element can be calculated (Edwards et al., 2021). measured the microplasticity in a lamellar TiAl alloy during high cycle tensile fatigue by high resolution digital image correlation strain mapping at several stress and cycle increments under different conditions. They suggested that for the design of advanced TiAl alloys for increased damage tolerance, a more uniform microplastic strain, accommodated by effective strain transfer at microstructural boundaries, is to be targeted.

However, our model does not require probability function to describe the microplastic behavior as (Jirandehi and Khonsari, 2021), the analysis of fluctuation local stress at critical plane as (Ustrzycka et al., 2020), or derivation of a transition function from microplastic to macroplastic flow response as (Mozafari et al., 2020). Instead, in this paper the calculation of microplasticity that lead to entropy production is more similar to the two scale model shown in (Teng et al., 2020a, 2020b, 2020c). Nevertheless, the total intrinsic dissipation is derived on pure physics instead of doing the experimental thermal analysis.

In section 2, of this paper the unified mechanics theory is briefly introduced for readers who are not familiar with the theory. In section 3, thermodynamic fundamental equation is derived. More details of our microplasticity calculation will also be presented in this section. In section 4, the damage evolution formula is introduced and implemented in a MATLAB code to predict the fatigue life of a metal specimen under a high cycle fatigue. Simulation results are compared with test data.

2. Unified mechanics theory

Details of this theory are provided in (Basaran, 2021). Herein we provide a very brief introduction. In Newtonian mechanics-based theory of elasticity, there is no dissipation, degradation mechanism, or irreversible process [entropy generation]. In theory of elasticity, it is assumed that deformation is reversible and the mechanism is 100% efficient from thermodynamic perspective. For example, according to Hooke's Law, the strain of a spring of stiffness k subjected to load F is given by, $\varepsilon = \Delta l/l_0$, $\Delta l = F/k$. This strain is independent of age of the spring. In other words, if we consider spring as a thermodynamic system. It is assumed that efficiency of the system is 100%, which is a violation of the 2nd law of the thermodynamics.

However, it is well known that under a cyclic loading in linear elastic regime, any metal will still fatigue. Therefore, clearly the second law of thermodynamics is not violated. There is always irreversible entropy generation in any closed system, which is ignored in the Newtonian mechanics based theory of elasticity. If we apply a cyclic load on a metal within its elastic range [below the yield stress], the corresponding strain would always be the same at every cycle, according to the theory of elasticity. Because the second law of thermodynamics is not included in the universal laws of Newton directly. In summary, there is no entropy term or TSI axis in the formulation of the universal laws of motion by Newton. Moreover, in Newtonian mechanics the laws of thermodynamics are satisfied separately than laws of Newton [not in the same differential equation], (such as, satisfying the thermodynamic consistency using the Clausius-Duhem inequality). As a result, in Newtonian continuum mechanics derivative of displacement with respect to entropy is zero. In simple terms, for example Newton's second law $a = F/m$ gives initial acceleration of a ball. Laws of thermodynamics must be used and formulated separately to calculate the distance ball will travel. In unified mechanics this information is automatically included in the second law of the unified mechanics theory. No separate calculation is needed.

The concepts of thermodynamics can be traced back to 1850, when Rudolf Clausius (1850) and William Thompson (Kelvin) (Thomson, 1853) formulated both the first and second laws of thermodynamics. The first law is the conservation of energy. The second law is the entropy law. It states that in a natural process, the sum of the entropies of the interacting systems increases; The entropy of an isolated system never decreases. That is, there is a natural tendency of any isolated system, living or non-living, to degenerate into a more disordered state. When irreversible entropy generation rate becomes zero the system reaches thermodynamic equilibrium. If we regard the specimen as a thermodynamic system, when irreversible entropy generation rate becomes zero the specimen fails, (Basaran, 2021; Callen, 1985).

In statistical mechanics, entropy is an extensive property of a thermodynamic system. It is related to the number of microstructural configurations (a.k.a microstates) that are consistent with the macroscopic quantities and boundary conditions that characterize the system. The logarithmic connection between entropy and disorder state was first stated by L. Boltzmann in 1877 (Boltzmann, 1877) and put into final form by Max Planck in 1900 (Planck, 1900). The statistical interpretation of entropy is given by

$$S = k_B \ln \mathrm{W} \tag{2}$$

In which S is the entropy, k_B is the Boltzmann constant and W is the disorder parameter. Entropy of any system can be calculated from thermodynamic fundamental equation, (Basaran, 2021) (Callen, 1985). The second law states that in any isolated system W has a natural tendency to evolve into a more disordered state. When maximum disorder is reached, the system is in thermodynamic equilibrium.

In unified mechanics theory laws of Newton and laws of thermodynamics are unified at ab-initio level. As a result in addition to Newtonian x, y, z, time coordinates system, there is an additional fifth axis called Thermodynamic State Index (TSI) axis, which is linearly independent. As a result, derivative of displacement with respect to entropy is not zero as in Newtonian mechanics. In unified mechanics theory, in addition to nodal displacements, the entropy generation rate is also necessary at each increment to relate microstructural changes in the material with spatial and temporal coordinates.

After formalizing the concepts described above mathematically, Newton's second and third laws are unified with the second law of thermodynamics. Following laws of the unified mechanics theory are established (Basaran, 2021)

$$\text{The second law,} \quad (1-\phi)F\,dt = d(mv) \tag{3}$$

$$\text{The third law,} \quad F_{12} = \frac{d\left[\frac{1}{2}k_{21}u_{21}^2(1-\phi)\right]}{du_{21}} \tag{4}$$

where, ϕ is TSI, F_{12} is the acting force, k_{21} and u_{21} are the stiffness and change in length of the reacting system.

Thermodynamic State Index (TSI), ϕ, is given by

$$\phi = \phi_{cr}\left[1 - \exp\left(-\Delta s \frac{m_s}{R}\right)\right] \tag{5}$$

where

$$\phi_{cr} = \frac{\phi}{Factor\ of\ safety} \tag{6}$$

In equations (5) and (6), ϕ_{cr} is a user-defined critical value of TSI, Δs is the change in specific entropy, m_s is the molar mass, and R is the gas constant. When a material is in ground (reference) state, it is assumed to be free of any possible defects. It can be assumed that "damage" in a material is equal to zero. Therefore, TSI will be $\phi = 0$. However, ϕ does not have to be taken as zero initially. In the final stage, material reaches an asymptotic thermodynamic equilibrium state. At this stage, entropy production rate will become zero, and $\phi = \phi_{cr}$. The purpose of ϕ_{cr} is to adequately capture the specimen's critical states of interest. For example, in the electromigration analysis of microelectronics solder joint, $\phi_{cr} = 0.10$ is used because 10% change in electrical resistance is considered failure in microelectronics, (Basaran et al., 2009). Unlike electromigration analysis of the solder joints, we set this ϕ_{cr} value to a pre-defined value or simply set it as 1 for the fatigue analysis.

Fig. 1 shows the coordinate system in the unified mechanics theory. It is important to emphasize that in the new coordinate system derivative of displacement with respect to entropy is not zero because TSI is a linearly independent axis.

Since, 1998 (Basaran and Yan, 1998) the concept of using entropy as a damage metric to predict fatigue life has been extensively used for thermal, mechanical electrical loading and corrosion-fatigue, but never for high cycle fatigue [linear-elastic loading] (Basaran and Lin, 2008),-(Li et al., 2009), (Basaran et al., 2004a, 2004b, 2008, 2009; Basaran and Yan, 1998; Basaran and Nie, 2004; Yao and Basaran, 2012, 2013a, 2013b, 2013c; Basaran and Lin, 2007a, 2007b; Ye et al., 2004, 2006; Li et al., 2008a, 2008b; Mankarathodi et al., 2020; Temfack and Basaran, 2015; Basaran and Chandaroy, 2000; MehdizadehAli and Khonsari, 2021; Hajshirmohammadi and Khonsari, 2020; Imanian and Modarres, 2015; Wang and Yao, 2017, 2019; Young and Subbarayan, 2019; Yun and Modarres, 2019a, 2019b; Osara and Bryant, 2019; Egner et al., 2020; Ribeiro et al., 2020; Teng et al., 2020b; Naderi et al., 2010). Mathematical details of the unified mechanics theory (UMT) are available in the literature, hence, we do not find it necessary to provide any further details.

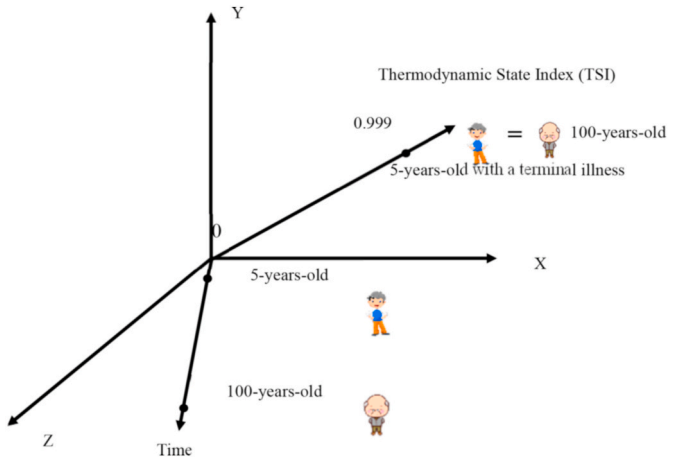

Fig. 1. Coordinate system in unified mechanics theory (Basaran, 2021),.

3. Derivation of thermodynamic fundamental equation for high cycle fatigue: Entropy generation mechanisms

The following assumptions are made in the study.

1. Applied maximum stress is below the yield stress of the material hence no macroscopic plastic deformation is expected.
2. A mechanism called micro-plasticity is expected to happen at some defect sites at micro-level (Lemaitre et al., 1999; Doudard et al., 2005; Charkaluk and Constantinescu, 2009; Fan et al., 2018).
3. Point defects, including atomic vacancies, interstitials, and impurities, can be built-in with the original crystal growth or created by energy input during fatigue process.
4. Input mechanical energy increases atomic vacancies and dislocation densities. However, the increasing dislocation density only causes hardening in the micro-level and never induces macroscopic plastic deformation as the maximum applied stress is below the metal's yield stress. The vacancy generation/diffusion and dislocation motions(e.g. cross slip) around inclusions induce irreversibility at a micro-level in elastic cyclic loads, (Callister and Rethwisch, 2018; Marti et al., 2020; Mughrabi, 2009, 2013; Ho et al., 2017).
5. Vacancy concentration gradient in the specimen will result in vacancy diffusion and temperature gradient in the specimen result in thermomigration.
6. Temperature evolution in the specimen is determined by atomic-friction-generated heat, heat conduction, microplastic work and thermoelastic damping.

3.1. Configurational entropy generation

The micro-mechanisms in the crystal include the rearrangement of atoms which result in entropy production during the elastic fatigue loading, (Kelly et al., 2012) (Abbaschian and Reed-Hill, 2009).

Starting from Boltzmann's entropy equation for entropy $S = k_B \ln W$ (Boltzmann, 1877) (Planck, 1900), in which k_B is the Boltzmann constant and W is disorder parameter that describes the probability that the system will exist in the state it is in relative to all the possible states it could be in (Basaran, 2021) (Planck, 1900) (Basaran and Nie, 2004). We note that actually, this form of the Boltzmann equation is due to Plank (Planck, 1900). The configurational entropy S_c is a concept from statistical thermodynamics that use the binomial distribution formula (N is the number of lattice sites and n is the number of vacancies) $\frac{N!}{(N-n)!n!}$ to replace the disorder parameter W, which is derived in the following form (Boltzmann, 1877) (Kelly et al., 2012) (Abbaschian and Reed-Hill, 2009) (Planck, 1900):

$$S_c = k_B \ln\left(\frac{N!}{(N-n)!n!}\right) \tag{7}$$

Atomic vacancies, defects, result from missing atoms from their original lattice sites. These vacancies are rearranged due to the thermally activated transport. The variation of ΔS_c from temperature state 1 to temperature state 2 is given by,

$$\Delta S_c = k_B \ln\left(\frac{N!}{(N-n_2)!n_2!}\right) - k_B \ln\left(\frac{N!}{(N-n_1)!n_1!}\right) \tag{8}$$

where n_1 and n_2 are the number of vacancies at temperature state 1 and state 2, respectively. Equation (8) can further be derived into the following form

$$\Delta S_c = k_B N\left[C_{v2} \cdot \ln\left(\frac{1-C_{v2}}{C_{v2}}\right) - C_{v1} \cdot \ln\left(\frac{1-C_{v1}}{C_{v1}}\right)\right] \tag{9}$$

In which C_{v1} and C_{v2} are the thermodynamic equilibrium vacancy concentration at temperature state 1 and state 2, respectively.

3.2. Vibrational entropy generation

The vibrational entropy is also a concept from statistical thermodynamics [or physical chemistry] that replaces disorder parameter W with the phase state of the atoms as they vibrate, which is defined by momentum and position coordinates (Fultz, 2010) (Atkins Paulaet al, 2018; Wollenberger, 1996; Laughlin and Hono, 2014). The vibrational state of the atoms change when vacancies are created. There are various models proposed to precisely calculate vibrational entropies when certain number of vacancies are removed, (Mishin et al., 2001). In this research we simply assume the variation of vibrational entropy is the same when each atomic vacancy is created (Abbaschian and Reed-Hill, 2009) (Burton, 1972). Therefore the total vibrational entropy in the system is given by,

$$S_{vib} = n\Delta S_v \tag{10}$$

In which n is the number of vacancies created and ΔS_v is the variation of vibrational entropy when one atomic vacancy is created.

The variation ΔS_{vib} is

$$\Delta S_{vib} = (n_2 - n_1)\Delta S_v \tag{11}$$

Comparing configurational entropy and vibrational entropy magnitudes.

The parameters necessary to calculate the configurational and vibrational entropy magnitudes are listed in Table 1.

Entropy calculations for these two mechanisms are based on the number of vacancies [or the vacancy concentration], which is related to the temperature at that state. If we assume that after several cycles, temperature in the metal increases from $T_0 = 298K$ to $T_i = 398K$, we can calculate the evolution of ΔS_c and ΔS_{vib}. Fig. 2, shows configurational entropy as a function of temperature. Fig. 3, shows vibrational entropy as a function of temperature.

3.3. Entropy generation due to vacancy concentration gradient driven diffusion

During fatigue process concentration of vacancies in the metal are not uniform. As a result, there is a vacancy concentration gradient. Vacancy concentration gradient driven diffusion and thermo-migration are governed by the vacancy conservation equation (or mass conservation), (Basaran and Lin, 2007a; Ye et al., 2004, 2006). Concentration of atomic vacancies should be higher around the edge and lower around the center for specimen with a round cross-section (cracks usually develop from outside to inwards), hence cause the vacancy diffusion.

The entropy generation from vacancy gradient driven diffusion ΔS_d is extensively studied (Basaran and Lin, 2008),- (Li et al., 2009), (Basaran et al., 2004a, 2004b, 2008; Basaran and Lin, 2007b; Li et al., 2008b; Yao and Basaran, 2013a, 2013b, 2013c). It is given by:

$$\Delta S_d = \int_{t_0}^{t} \left(\frac{C_v D_v}{k_B T^2} \left(\frac{Q^* \nabla \mathrm{T}}{T} + \frac{k_B T}{c} \nabla c \right)^2 \right) dt \tag{12}$$

where k_B is the Boltzmann constant, C_{v0} is the thermodynamic equilibrium vacancy concentration in the absence of a stress field, C_v is instantaneous atomic vacancy concentration, c is normalized vacancy concentration $c = C_v/C_{v0}$, D_v is effective vacancy diffusivity, T is absolute temperature, Q^* is heat of transport, which is the isothermal heat transmitted by the moving atom in the process of jumping a lattice site.

To compare the order of magnitude of equation (12) with other entropy generation mechanisms, following condition is assumed:

The specimen is initially placed at room temperature (298 K). After several cycles, the temperature at specimen's gage section is uniformly

Table 1
Parameters to calculate configurational and vibrational entropy.

Parameters		value	units
Avogadro's number	N_A	6.023×10^{23}	$atoms/mol$
Atomic weight	A_{wFe}	55.85	g/mol
Density of steel	ρ_{steel}	7.894	g/cm^3
Vacancy formation energy for Fe	Δh_f	1.08	eV
Boltzmann constant	k_B	8.62×10^{-5}	eV/K
		1.38×10^{-23}	J/K
Vibrational entropy for bcc crystals	Δs_v	2.4	$k_B/atom$

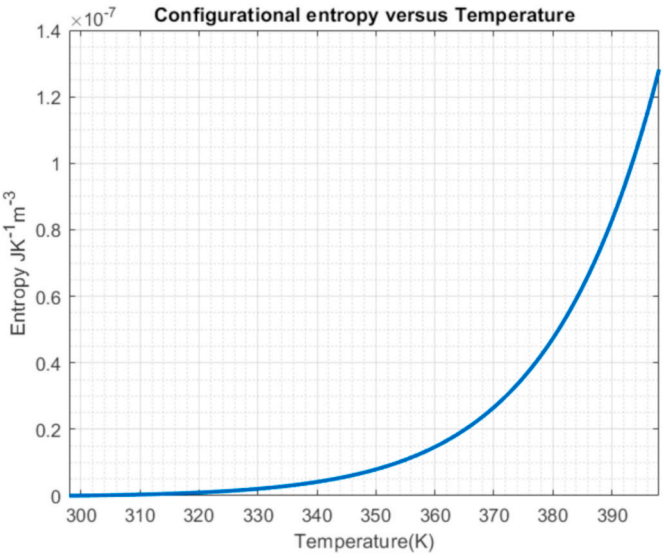

Fig. 2. Configurational entropy($JK^{-1}m^{-3}$) versus temperature evolution.

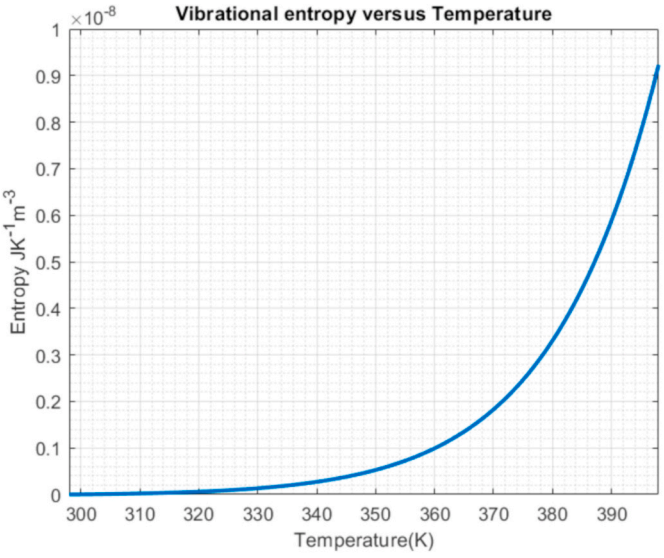

Fig. 3. Vibrational entropy ($JK^{-1}m^{-3}$) versus temperature evolution.

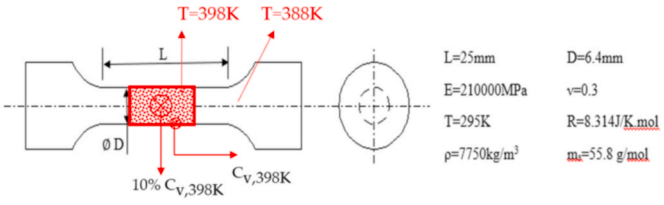

Fig. 4. an illustration of vacancy gradient.

increased to 398 K. We assume the vacancy concentration at the center is ten times smaller than at the edge, Fig. 4. The thermodynamic equilibrium vacancy concentration C_v can be calculated by

$$C_v = \exp\left(\frac{T\Delta S_v - \Delta h_f}{k_B T}\right) \tag{13}$$

The vacancy concentration at room temperature (298 K) and at 398 K can be obtained as follows

$$\begin{aligned} C_{v,\ 398K} &= 2.35 \times 10^{-13} \\ C_{v0} &= C_{v,\ 298K} = 6.1 \times 10^{-18} \end{aligned} \tag{14}$$

The normalized vacancy concentration c and normalized vacancy gradient are therefore given by

$$\begin{aligned} c_{\ edge} &= \frac{C_{v,\ 398K}}{C_{v0}},\ c_{\ center} = \frac{0.1C_{v,\ 388K}}{C_{v0}} \\ \nabla c &= \left(c_{\ edge} - c_{\ center}\right)/1cm = 3.5 \times 10^6 m^{-1} \end{aligned} \tag{15}$$

The effective vacancy diffusivity D_v is given by

$$D_v = D_0 \exp\left(\frac{-Q}{RT}\right) \tag{16}$$

For BCC iron (α-Fe), $D_0 = 2.8 \times 10^{-4}\frac{m^2}{s}$, activation energy $Q = 251kJ/mole$, $R = 8.3145\frac{J}{mole\ K}$ (Brandes and Brook). At 398 K, $D_v = D_0 exp\left(\frac{-Q_d}{RT}\right) \approx 3 \times 10^{-37}\frac{m^2}{s}$.

We can calculate the value of equation (12) as follows

$$\begin{aligned} \dot{S}_d &= \frac{2.35 \times 10^{-13} \times 3 \times 10^{-37}\frac{m^2}{s}}{1.38 \times 10^{-23} J/K \times (398K)^2}\left(\frac{1.38 \times 10^{-23} J/K \times 398K}{3852} 3.5 \times 10^6 m^{-1}\right)^2 \\ &= 8 \times 10^{-91} JK^{-1}s^{-1} \end{aligned} \tag{17}$$

From the result of equation (17), it can be concluded that the entropy generation due to mass transport is negligible compared to other mechanisms.

3.4. Entropy generation due to heat conduction

In metal high cycle fatigue, a temperature gradient in the specimen which causes an irreversible heat flow across different temperature field is usually expected (Xue et al., 2008). The entropy generation equation is given by (Basaran, 2021) (Teng et al., 2020a), (Basaran et al., 2004b, 2008; Basaran and Lin, 2007b; Li et al., 2008b; Yao and Basaran, 2013a, 2013b, 2013c)

$$\Delta S_T = -\int_{t_0}^{t}\left(k_h \frac{\nabla T \cdot \nabla T}{T^2}\right)dt \tag{18}$$

where k_h is coefficient of heat conduction, ∇T is the temperature gradient. Again, in order to calculate the order of magnitude of this entropy generation mechanism, we assume a simple one dimensional temperature gradient $\frac{\Delta T}{\Delta x} = 10\,K/_{cm}$ from the gage section to the grip section, Fig. 4. The thermal conductivity of steel is $K_h = 50\frac{W}{K \cdot m}$. After several cycles, if the temperature increases from $T_0 = 298K$ to $T_i = 398K$, and then maintain steady until near failure at around 1.4×10^5 cycles(operating frequency at 30 Hz). The evolution of ΔS_T for a specimen is shown in Fig. 5.

3.5. Entropy generation due to atomic-friction (scattering)-generated heat

The entropy generation due to atomic-friction-generated heat is given by (Basaran, 2021) (Callen, 1985) (Basaran and Nie, 2004)

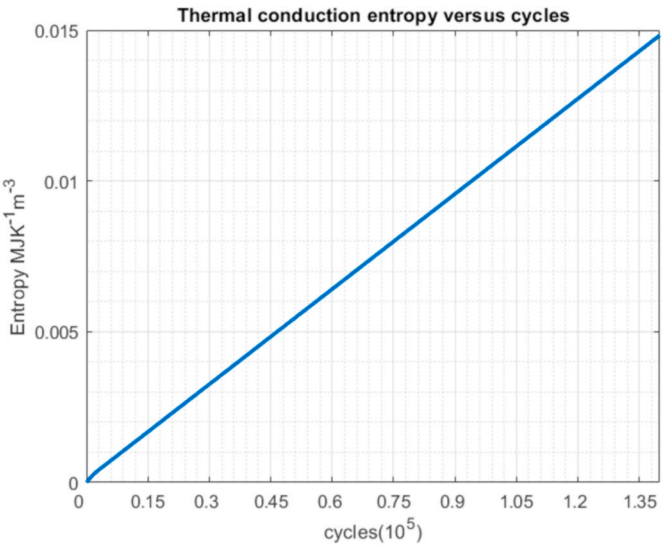

Fig. 5. Entropy production due to thermal conduction ($JK^{-1}m^{-3}$) versus number of cycles.

$$\Delta S_r = \int_{t_0}^{t}\frac{\rho r}{T}dt \tag{19}$$

From microscopic perspective, temperature is defined by the intensity of atomic vibrations. The atomic-friction-generated heat per unit mass, r, is due to the increasing intensity of atomic vibrations in the crystal from micro-mechanisms such as the breaking of atomic bonds, and phonon-phonon scattering, phonon-electron-scattering, electron scattering (called internal friction), (Gao, 1876) (Ragab and Basaran, 2009) (Chu et al., 2015). This term is essentially different than the heat generated through the macroscopic observable plastic work or thermoelastic source.

Molecular dynamics simulation are used estimate the internal heat generation due to internal frictions. Using LAMMPS (Plimpton, 1995), a simulation cell with 10 lattice units in each direction for a total of 2000 Fe atoms are arranged in bcc crystal structure. Periodic boundary condition is chosen. The embedded-atom method (EAM) is used to compute the pairwise interactions. Atomic bond potential is obtained from (Chamati et al., 2006). At the equilibrium step, the lattice is allowed to relax to achieve a system temperature of 300 K and a pressure of 0 kbar at each cell boundary under the NPT ensemble. Then during the deformation step, a "deform" command is applied to the simulation cell in the x-direction at strain rates of 0.001/pico-second, 0.005/pico-second and 0.01/pico-second under uniaxial compression and tension. The NVE ensemble chosen in this step in order to achieve an isolated system.

The NVE ensemble controls the conservation of total energy in the system while allowing the system temperature to change under applied deformation. The increase of the intensity of atomic vibrations due to the breaking of atomic bonds can be captured by the temperature evolution. Results of temperature evolution with respect to strain is shown in Fig. 6 and Fig. 7.

In Figures (Basaran and Lin, 2008; Li et al., 2009), it is shown that the temperature fluctuation during uniaxial compression and tension are not completely reversible at higher strain rates and deformation ratio (e.g. for 0.01/picosecond at 20 ps). As a result, temperature increases by 250 K for compression but decreases 90 K for tension. However, at lower strain rate and lower deformation ratio, the temperature fluctuation is negligible (e.g. for strain rates below 0.001/ps). It is therefore concluded that at low strain rates, the temperature fluctuation is solely the result of thermoelastic coupling. Atomic-friction-generated heat is negligible and can be neglected below 0.001/picosecond rate of loading.

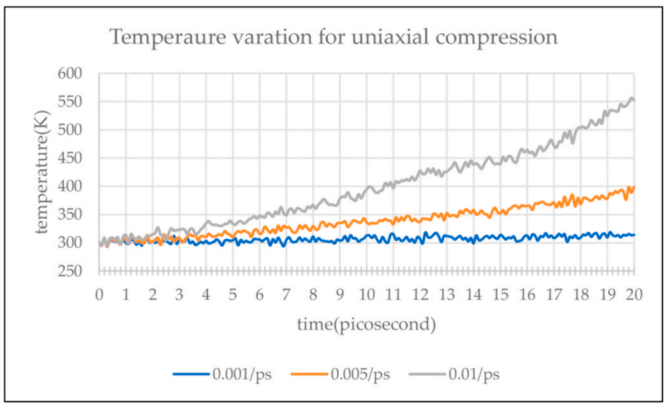

Fig. 6. Temperature variation with time under uniaxial compression under different strain rates.

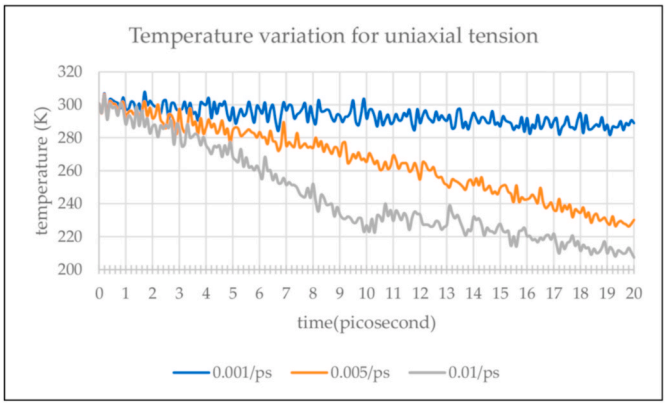

Fig. 7. Temperature variation with time under uniaxial tension for different strain rates.

3.6. Entropy generation due to micro-plasticity

The term micro-plasticity is used in two scale models, which was initially developed by (Lemaitre et al., 1999) and then reformulated by Doudard (Doudard et al., 2005). These researchers developed the micro-plasticity model to calculate the amount of micro-plastic strain during a high cycle fatigue. Then used the micro-plastic strain as a variable in an empirically function obtained from test data to predict the fatigue life. In our study micro-plastic strain is needed just to be able to calculate the entropy generation. We do not to use it as a variable in an empirical curve-fit function to predict the fatigue life.

The fatigue regime in the material is investigated at macroscopic and microscopic scales independently. From the macroscopic view the material is deformed elastically during the elastic cyclic fatigue loading while from the microscopic view some micro-plasticity is activated because of high stress concentration at defects and localized dislocation slip planes (Lemaitre et al., 1999; Doudard et al., 2005; Charkaluk and Constantinescu, 2009; Fan et al., 2018).

The two scale model is based on a RVE (Representative Volume Element) and divides it into two parts: elastic matrix part and elastic-plastic inclusion part (see Fig. 8). The law of localization and homogenization is applied to deduce the relationship between macroscopic stress tensor and the microscopic stress and microscopic plastic strain tensors (Lemaitre et al., 1999) (Doudard et al., 2005) (Fan et al., 2018).

Microscopic stress tensor is given by,

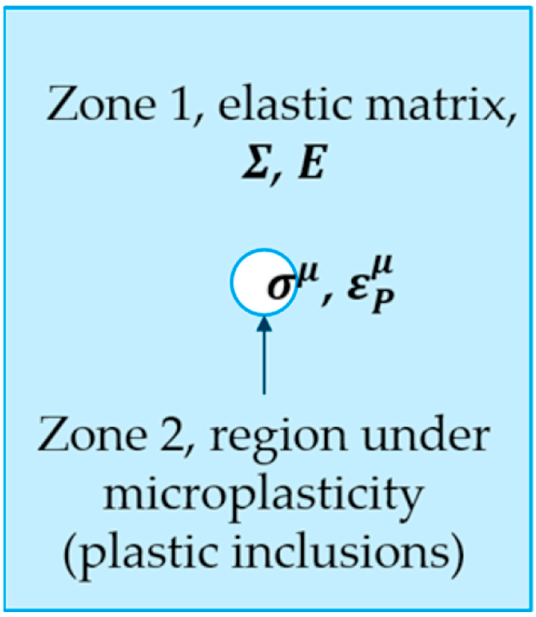

Fig. 8. A representative volume element of the two scale model, $\boldsymbol{\Sigma}$ is macroscopic elastic stress tensor, $\boldsymbol{E}$ is macroscopic elastic strain tensor, $\boldsymbol{\sigma}^{\mu}$ is microscopic stress tensor, $\boldsymbol{\varepsilon}_p^{\mu}$ is microscopic plastic strain tensor.

$$\boldsymbol{\sigma}^{\mu} = \boldsymbol{\Sigma} - 2\mu(1-b)\boldsymbol{\varepsilon}_p^{\mu}$$
$$b = \frac{6(K+2\mu)}{5(3K+4\mu)} \tag{20}$$

where $\boldsymbol{\sigma}$ is microscopic stress tensor, $\boldsymbol{\Sigma}$ is macroscopic stress tensor, μ is the Lame's constant, K is bulk modulus and $\boldsymbol{\varepsilon}^{p}$ is microscopic plastic strain tensor.

(Charkaluk and Constantinescu, 2009) derived a modification of equation (20) using Kroner's self-consistent scheme (Kröner, 1961). In the case of isotropic elastic behavior with a classically defined deviatoric plasticity, one can write the following relation,

$$\boldsymbol{\sigma}^{\mu} = \boldsymbol{\Sigma} - 2\mu(1-b)(1-f_v)\boldsymbol{\varepsilon}_p^{\mu} \tag{21}$$

where f_v is the volume fraction of micro-defects experiencing micro-plasticity. Assuming that the material experiences the same elastic behavior at the mesoscopic and the macroscopic scale, the previous relation implies,

$$\boldsymbol{\varepsilon}_e^{\mu} = \boldsymbol{E} - [(1-b)(1-f_v)]\boldsymbol{\varepsilon}_p^{\mu} \tag{22}$$

where $\boldsymbol{\varepsilon}_e^{\mu}$ is the microscopic elastic strain tensor.

Charkaluk and Constantinescu (2009) report that, although it cannot exactly be correlated to the volume ratio, it is assumed that the relative surface ratio covered by the activated micro slip bands can be used to represent f_v. For a low carbon steel which has a fatigue limit of 235 MPa, a value of $f_v = 3\%$ is chosen for a stress amplitude of 180 MPa, a value of $f_v = 10\%$ for a stress amplitude of 250 MPa and a value of $f_v = 20\%$ for a stress amplitude of 300 MPa. However, these numbers taken from (Cugy et al., 2002) are purely empirical. We believe f_v may be calculated by dislocation dynamics simulations for a given initial defect ratio.

A computational scheme for the microplastic strain increment was proposed by Charkaluk and Constantinescu (2009), as follows

$$\Delta\boldsymbol{\varepsilon}_p^{\mu} = \frac{\sqrt{\frac{3}{2}}\boldsymbol{A}_{n+1}^{*} - \sigma_{y0}^{\mu}}{\sqrt{\frac{3}{2}}\left(2\mu(1-b)(1-f_v) + \frac{2}{3}\mathrm{h}\right)} \frac{\boldsymbol{A}_{n+1}^{*}}{\boldsymbol{A}_{n+1}^{*}} \tag{23}$$

In which h is the hardening modulus, and $\boldsymbol{A}_{n+1}^{*}$ is given by,

$$\boldsymbol{A}^{*}_{n+1} = \mathrm{dev}(\boldsymbol{\Sigma}_{n}) - \left(2\mu(1-b)(1-f_v) + \frac{2}{3}\mathrm{h}\right)\boldsymbol{\epsilon}^{\mu}_{p,n} + dev(\Delta\boldsymbol{\Sigma}) \qquad (24)$$

$$b = \frac{6(K+2\mu)}{5(3K+4\mu)}$$

For the microplasticity model, linear kinematic hardening is utilized as a first approximation. The yield criterion is given by,

$$f = \sqrt{(\boldsymbol{S}^{\mu} - \boldsymbol{\alpha}^{\mu d}) : (\boldsymbol{S}^{\mu} - \boldsymbol{\alpha}^{\mu d})} - \sqrt{\frac{2}{3}}\sigma^{\mu}_{y0} = 0 \qquad (25)$$

and the hardening rule is given by

$$\dot{\boldsymbol{\alpha}}^{\mu} = h\dot{\boldsymbol{e}}^{\mu p}\frac{1}{\sigma^{\mu}_{y0}}(\boldsymbol{\sigma}^{\mu} - \boldsymbol{\alpha}^{\mu}) = h\sqrt{\frac{2}{3}\dot{\epsilon}^{\mu p}_{ij}\,\dot{\epsilon}^{\mu p}_{ij}}\;\frac{1}{\sigma^{\mu}_{y0}}(\boldsymbol{\sigma}^{\mu} - \boldsymbol{\alpha}^{\mu}) \qquad (26)$$

where $\boldsymbol{S}^{\mu}$ is the microscopic deviatoric stress, $\boldsymbol{\alpha}^{\mu d}$ is the deviatoric part of the microscopic back stress, $\boldsymbol{e}^{\mu p}$ is the microscopic equivalent plastic strain, σ^{μ}_{y0} is the microscopic yield stress, $\boldsymbol{\sigma}^{\mu} - \boldsymbol{\alpha}^{\mu}$ is the translational direction of the microscopic yield surface under Ziegler's rule, h is the kinematic linear hardening modulus defined as the slope of the stress strain curve for a finite plastic strain value, $h = (\sigma^{\mu} - \sigma^{\mu}_{y0})/\,\varepsilon^{\mu p}$.

The entropy generation due to microplasticity is given by (Basaran, 2021) (Basaran and Yan, 1998) (Basaran and Nie, 2004) (Mankarathodi et al., 2020) (Basaran et al., 2004a).

$$\Delta S_{\mu p} = \int_{t_0}^{t} \phi f_v \frac{\boldsymbol{\sigma}^{\mu} : \dot{\boldsymbol{\epsilon}}^{\mu}_{p}}{T} dt \qquad (27)$$

In which $\boldsymbol{\sigma}^{\mu}$ and $\dot{\boldsymbol{\epsilon}}^{\mu}_{P}$ are micro stress and strain rate tensors. During the microscopic plastic deformation, some plastic work is stored as dislocation stored energy. This stored dislocation energy is accounted for in the hardening of the material, which is included in equation (26), and shown in Fig. 11.

In equations (21)–(24), (27), f_v is a constant that establishes a relation between the macro-stresses and micro-stresses by means of the law of localization and homogenization. It is the ratio of the activated volume of the micro-defects in region V_D to the elastic matrix V_{matrix}, (Charkaluk and Constantinescu, 2009) (Chamati et al., 2006). In the microplasticity model used here terms defect and dislocation are used for the same thing.

$$f_v = \frac{V_D}{V_{matrix}} \qquad (28)$$

In the microplasticity model we are using, f_v is defined as the maximum percentage of dislocation planes that can be activated (Doudard et al., 2005) (Charkaluk and Constantinescu, 2009) (Cugy et al., 2002). This value can be determined by using the Scanning Electron Microscopy (SEM), as shown in Fig. 10, or by other microscopy techniques.

In this study, we use the percentage of the observed active slip bands' area in the center of specimen's gauge part, as a first approximation to the volume fraction of defects (dislocations) in the matrix, $V_D/\,V_{matrix}$. Fig. 9 shows the Illustration.

Fig. 9 shows the illustration of microplasticity. Inside the hexagon region, microscopic stress and microplastic strain at each inclusion are computed using the laws of localization and homogenization.

3.6.1. Calculating entropy due to micro-plasticity

In the following section, material constants for simulation are obtained from (Charkaluk and Constantinescu, 2009) (Torabian et al., 2017), and are given in Table 2.

The microscopic yield stress in this microplasticity model (Charkaluk and Constantinescu, 2009) (Torabian et al., 2017) is the mean fatigue limit of the specimen. It is assumed that no microplasticity occurs below the macroscopic fatigue limit, (Lemaitre et al., 1999).

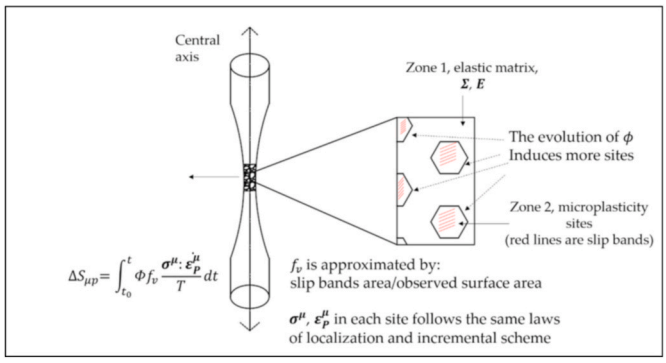

Fig. 9. Illustration of microplasticity entropy calculation.

Table 2
Material parameters for DP600 steel (Charkaluk and Constantinescu, 2009) (Torabian et al., 2017).

Youngs modulus	210000 MPa	Macroscopic yield stress	440 MPa
Hardening coefficients	1000 MPa	Microscopic yield stress	260 MPa
Poisson's ratio	0.3	Thermal expansion coefficient coefficientcoefficients	$10 \times 10^{-6}/°C$
Density	7894 kg m^{-3}	Heat capacity	460 J Kg^{-1}K^{-1}
		Time representative of the thermal exchanges, τ_{eq}	80s

The TSI, ϕ, in $\Delta S_{\mu p} = \int_{t_0}^{t} \phi f_v \frac{\sigma^{\mu}:\dot{\epsilon}^{\mu}_{P}}{T} dt$ is a metric of entropy evolution. It should be emphasized that f_v is not the percentage of coalesced cracks in the cross section. It is defined as the maximum percentage of dislocations slip planes that can be activated during microplasticity. We assume that the percentage of activated dislocations follow the evolution of thermodynamic state index.

Currently, we are unable to find any computational studies on the relation between f_v and stress amplitude. Moreover, there is no f_v data available obtained by microscopy for DP600 steel at hand. However (Torabian et al., 2017), performed a fatigue test on DP600 steel and published the results of fractography studies. The appearance of slip bands in ferrite grains on the surface of the specimen around gauge part under 30-Hz fatigue loading is shown in Fig. 10. The yellow arrows

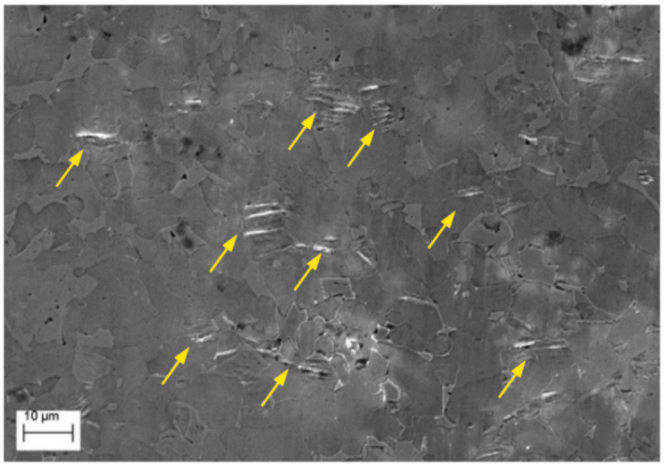

Fig. 10. Slip bands in ferrite grains on the surface of the specimen activated at 250 MPa stress amplitude. $N = 10^7$ cycles, $\Delta T < 15^{o}C$ [After (Torabian et al., 2017)].

indicates the slip bands, which are estimated to be around 10% of the observing surface. We use this $f_v = 10\%$ as a constant value for the calculation of stress and strain localizations in our study (Charkaluk and Constantinescu, 2009). report that the f_v value may be a material constant. However currently there is not enough experimental data to support this assumption. For specimen made of same material but with different geometry and dimensions, we believe that fractography studies for individual cases are necessary.

It should be noted that the microplasticity calculation in this subsection is based on the following assumptions:

1. The hardening behavior of the material is approximated by a bilinear kinematic hardening curve. Hardening modulus is defined as the slope between (lower yielding strength) LYS and UTS(ultimate tensile strength) from the stress strain curve, as a first approximation.
2. The microscopic hysteresis loops are stabilized and they are the same at each defect site. The evolution of TSI, ϕ, from 0 to 1 only induces microplasticity at more defect sites.
3. The energy dissipation due to kinematic hardening at microplasticity sites is small enough to be ignored (Naderi et al., 2010).

The hysteresis loop for one cycle at defect location calculated by equations 21–26 is shown in Fig. 11. The entropy production due to microplasticity for a specimen undergoing 1.4×10^5 cycles (at a frequency of 30 Hz) is shown in Fig. 12.

3.7. Comparison between different entropy generation mechanisms

The order of magnitude of each entropy generation mechanism is summarized in Table 3.

From Table 3, it is observed that the configurational entropy and vibrational entropy generation mechanisms are around the same order of magnitude. They are very small compared to heat conduction and microplasticity. The diffusion mechanism and atomic-friction-generated heat are also very small. Furthermore, between the microplasticity and heat conduction, entropy generation due to microplasticity is two orders of magnitude bigger. Hence, we conclude that the total entropy production, the thermodynamic fundamental equation, can be simplified as

$$\Delta S = \Delta S_{conf} + \Delta S_{vib} + \Delta S_d + \Delta S_T + \Delta S_r + \Delta S_{\mu p} \approx \Delta S_{\mu p} \tag{29}$$

Therefore, the thermodynamic state index of the unified mechanics theory can be given by,

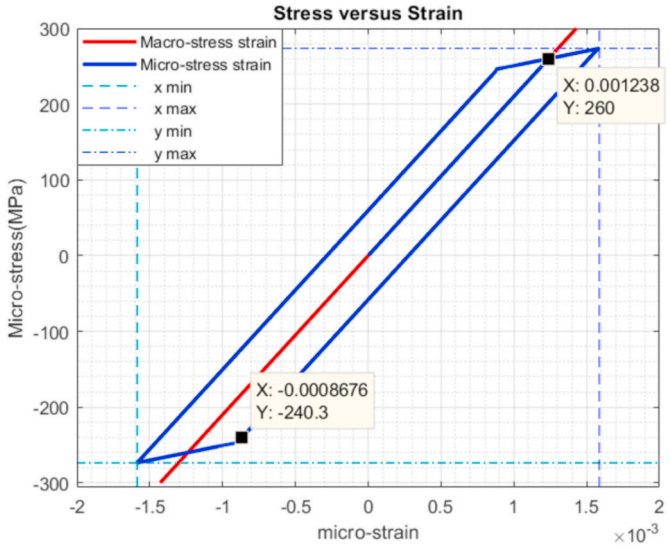

Fig. 11. Micro stress-strain curve for each individual inclusion (defect) site under 300Mpa nominal stress amplitude.

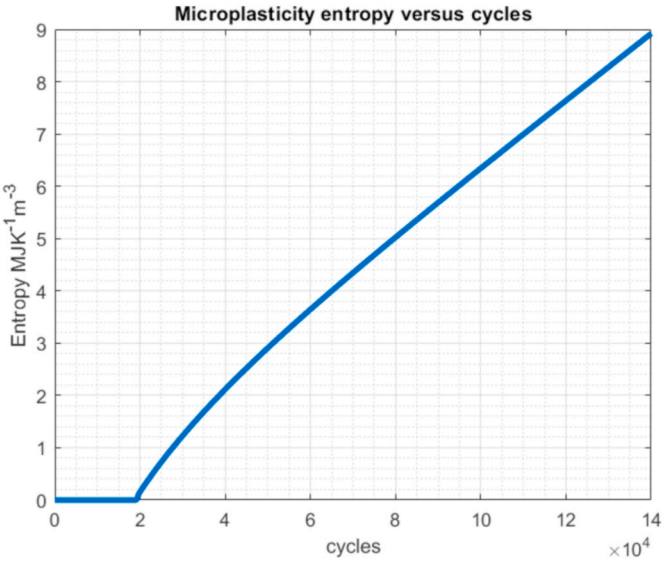

Fig. 12. Entropy generation($MJK^{-1}m^{-3}$) due to microplasticity versus number of cycles under 300 MPa nominal stress amplitude.

Table 3
Order of magnitude of different entropy generation mechanisms.

	Mechanisms	Magnitude of entropy generation
1	Configurational entropy	$\approx 10^{-7}$ $JK^{-1}m^{-3}$
2	Vibrational entropy	$\approx 10^{-8}$ $JK^{-1}m^{-3}$
3	Vacancy diffusion	Negligible due to low diffusivity
4	Thermal conduction	$\approx 10^{4}$ $JK^{-1}m^{-3}$
5	Atomic-friction-generated heat	Negligible based on molecular dynamics simulations
6	Micro-plasticity	$\approx 10^{6}$ $JK^{-1}m^{-3}$

$$\phi = \phi_{cr}\left(1 - \exp\left(\frac{-m_s \int_{t_0}^{t} \phi f_v \frac{\sigma^{\mu} : \dot{\varepsilon}_P^{\mu}}{\rho T} dt}{R}\right)\right) \tag{30}$$

In Equations (27) and (30) the reason to incorporate the TSI value into microplastic work is to account for the increasing probability of microdefects that emerge in the specimen during fatigue process.

Equation (30) is an exponential, hence, TSI never reaches unity. In practice we determine a ϕ_{cr} as a threshold. In this paper, we consider the specimen is failed when ϕ reaches $\phi_{cr} = 0.995$, since the probability of reaching maximum entropy at this state is 99.5%.

4. Temperature evolution due to mechanical work

The absolute temperature T of the specimen plays an import rule in metal high cycle fatigue life. We can expect to have different fatigue life prediction results if we control the temperature for the sample to achieve isothermal state. However, the degree of difference will depend on the isothermal temperature and thermodynamic equilibrium temperature of the sample. Because temperature gradient value controls the entropy generation rate in equations (12) and (18). Moreover, material properties are a function of temperature.

From the BCC ferrite grain point of view, the crack initiation mechanism can be divided to thermally activated mode and athermal mode. The transition between these two regimes is strongly dependent on strain rate and temperature (Torabian et al., 2017). For the high cycle fatigue of DP600 steel under conventional low frequency tension-compression loading (e.g. at 30 Hz) the strain rate is well below

the transition strain rate, for all ranges of stress amplitude. Hence the deformation is expected to happen in athermal region, where the formation of slip bands in ferrite grains results in local stress and strain concentration that leads to *trans*-granular crack initiation, eventually surface failure.

However, this is not always the case for high cycle fatigue under ultrasonic vibration because of the significantly higher degree of temperature rise due to self-heating and the high strain rate.

We can simulate the temperature evolution in equation (30) for more precise simulation. The absolute temperature of the specimen is governed by the fully-coupled thermo-mechanical equation derived from classical continuum mechanics as follows, (Basaran and Nie, 2004):

$$k_h \nabla^2 T = \rho C \dot{T} - \boldsymbol{\sigma} : \dot{\boldsymbol{\varepsilon}}^p - \rho r - T\left(\frac{\partial \boldsymbol{\sigma}}{\partial T} : \dot{\boldsymbol{\varepsilon}}^e\right) + \left(A_k - T\frac{\partial A_k}{\partial T}\right)\dot{V}_k \tag{31}$$

In which ρ is the density, $C = T\frac{\partial s}{\partial T}$ is defined as specific heat, $\boldsymbol{\varepsilon}^e$ and $\boldsymbol{\varepsilon}^P$ are elastic and plastic strain vectors, respectively, $\boldsymbol{\sigma}$ is the stress tensor, r is the strength per unit mass of the internal distributed heat source, and A_k is a thermodynamic force associated with the internal thermodynamic variables, V_k.

Equation (31) can yield the evolution of temperature due to mechanical work with properly imposed boundary conditions. In order to simplify this equation, we can ignore plastic strain $\dot{\boldsymbol{\varepsilon}}^p$, internal distributed heat source r and other thermodynamic variables $A_k \dot{V}_k$.

These assumption are justified, because.

1. We are investigating mechanical response under elastic loads only, as such there is no uniform plastic strain. However, the contribution from microplasticity is not neglected.
2. From section 3.5 we know the contribution of r is extremely small.
3. $\left(A_k - T\frac{\partial A_k}{\partial T}\right)\dot{V}_k$ represents the non-recoverable energy corresponding to internal coupling source (such as grain coarsening, phase transformation). However for metals this non-recoverable energy only represents 5–10% of the mechanical dissipation(plastic work) and is often negligible for high cycle fatigue (Naderi et al., 2010) (Teng et al., 2020c).

Therefore, equation (31) is simplified to the following expression

$$\rho C \dot{T} - \phi f_v \left(\boldsymbol{\sigma}^{\boldsymbol{\mu}} : \dot{\boldsymbol{\varepsilon}}_{\boldsymbol{P}}^{\boldsymbol{\mu}}\right) - k_h \nabla^2 T - T\frac{\partial \boldsymbol{\Sigma}}{\partial T} : \dot{\boldsymbol{E}}^e = 0 \tag{32}$$

If we ignore the thermal fluctuation due to thermoelastic damping, and simplify the conduction term as $-k_h \nabla^2 T \cong \rho C \frac{\theta}{\tau_{eq}}$, equation (32) can be written in the following time integration form

$$\begin{aligned} &\rho C \frac{T_{n+1} - T_n}{\Delta t} - \phi f_v \boldsymbol{\sigma}_{\boldsymbol{n}}^{\boldsymbol{\mu}} : \left(\frac{\boldsymbol{\varepsilon}_{\boldsymbol{P},\boldsymbol{n}+1}^{\boldsymbol{\mu}} - \boldsymbol{\varepsilon}_{\boldsymbol{P},\boldsymbol{n}}^{\boldsymbol{\mu}}}{\Delta t}\right) + \rho C \frac{T_n - T_0}{\tau_{eq}} = 0 \\ &T_{n+1} = T_n + \phi f_v \frac{\boldsymbol{\sigma}_{\boldsymbol{n}}^{\boldsymbol{\mu}} : \left(\boldsymbol{\varepsilon}_{\boldsymbol{P},\boldsymbol{n}+1}^{\boldsymbol{\mu}} - \boldsymbol{\varepsilon}_{\boldsymbol{P},\boldsymbol{n}}^{\boldsymbol{\mu}}\right)}{\rho C} - \frac{T_n - T_0}{\tau_{eq}} \Delta t \end{aligned} \tag{33}$$

Temperature evolution in the material is calculated at each cycle using equation (33).

The overall computation scheme is achieved in a coupled manner. We first assume a small starting ϕ value [use the equilibrium vacancy concentration] to calculate the microplastic work and TSI in the first step by equation (30), then use the obtained value to calculate the temperature increment in the next step by equation (33), and so on.

The entropy generated due to microplasticity is strongly affected by the stress amplitude. Fig. 13 shows the simulated temperature evolution for DP600 steel operating at 30 Hz for various stress amplitudes using equation (33). A rapid climbing stage followed by a steady state is observed. However, equation (33) cannot capture the rapid raising temperature when a specimen is near failure, when the temperature spikes.

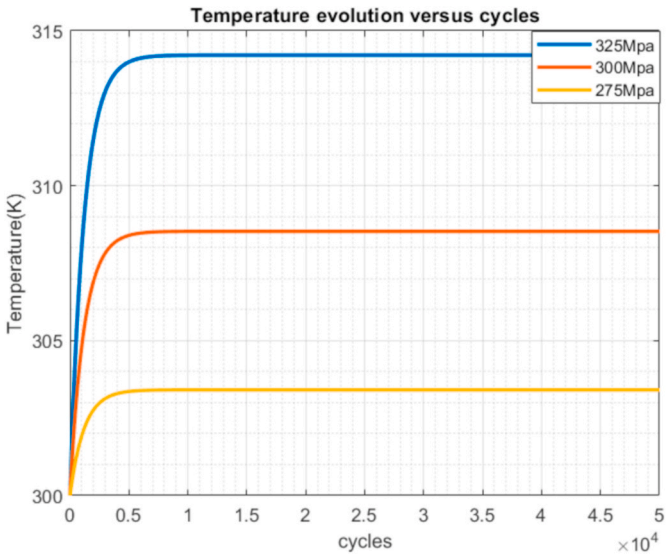

Fig. 13. Temperature evolution versus number of cycles at various stress amplitude.

Fig. 14 shows accumulated entropy at failure for various stress amplitudes. Accumulated total entropy at failure is also referred to Fatigue Fracture Entropy (FFE), which is known to be independent of stress amplitude (Yun and Modarres, 2019a).

Fig. 15 shows thermodynamic state index as a function of number of cycles. TSI, ϕ, reaches 1 around 8.5×10^4 cycles under 325 MPa applied stress. For stress amplitude of 300 MPa, TSI, ϕ reaches 1 at 1.4×10^5 cycles; For stress amplitude of 275 MPa, TSI, ϕ reaches 1 at around 3.6×10^5 cycles. It should be emphasized that if there are multiple notches/crack tips the sample will reach its fatigue failure entropy value [FFE] faster because there will be multiple stress concentration points and interactions among them, leading to a bigger entropy generation rate in the sample.

If we relate the stress amplitude with the number of cycles to failure, a bilinear curve can be plotted, Fig. 16.

In Fig. 14, we can observe that the TSI increases slowly in the early stage of cycling and suddenly begin to evolve rapidly after certain critical threshold. This trend can be explained by equation (32). In

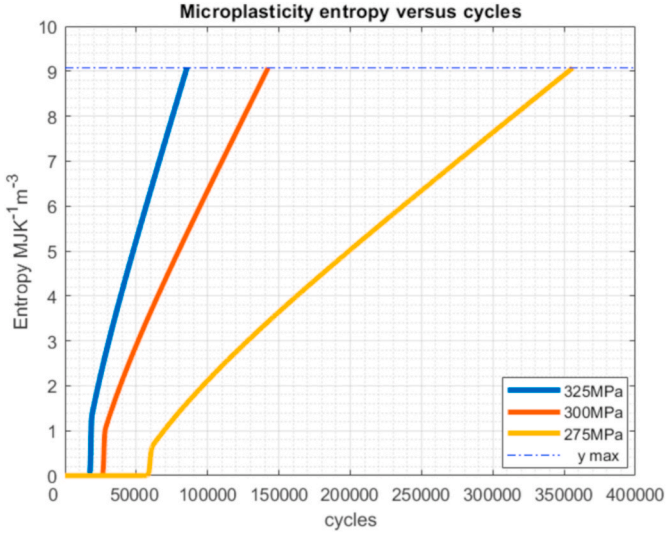

Fig. 14. Accumulated total entropy production versus number of cycles for various stress amplitudes. [This is also referred as the Fatigue Fracture Entropy].

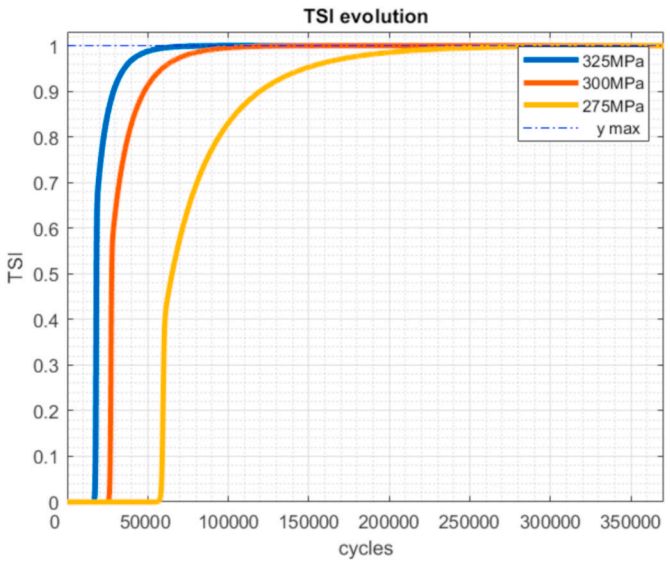

Fig. 15. TSI evolution versus number of cycles for various stress amplitudes.

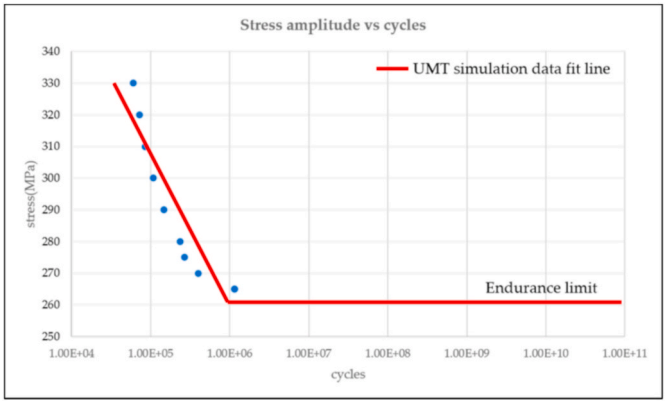

Fig. 16. Fatigue life prediction with UMT for stress amplitude versus number of cycles for various stress amplitudes. When TSI ϕ reaches $\phi_{cr} = 0.995$, the specimen is considered as failed.

equation (32), TSI is included in the equation of microplasticity entropy production to account for influence of microplasticity on entropy production. At the early stages there are too few microplasticity sites. Because microplasticity is the largest contributor to entropy generation, the corresponding TSI calculated by the entropy production is small at early stages. After a certain number of cycles, enough microdefects are activated hence more entropy is produced. The significant increase in entropy causes the sudden increase of TSI. This trend is similar to low cycle fatigue test data reported in the literature, (Mankarathodi et al., 2020) (Temfack and Basaran, 2015).

Simulation results obtained using the unified mechanics theory are shown in, Fig. 16, are compared with test data from (Torabian et al., 2017) are shown in Fig. 17. It shows that the predicted cycles to failure obtained from unified mechanics theory and the test data of (DP600) at 30 Hz loading frequency are matching reasonably well. Test data given in Fig. 17 shows expected scatter, especially at lower stress levels. It is very well known that fatigue test data is always stochastic. Unified mechanics theory, which is based on Boltzmann entropy formulation yields stochastic expected life.

5. Conclusions

Unified mechanics theory is used for predicting high cycle fatigue life

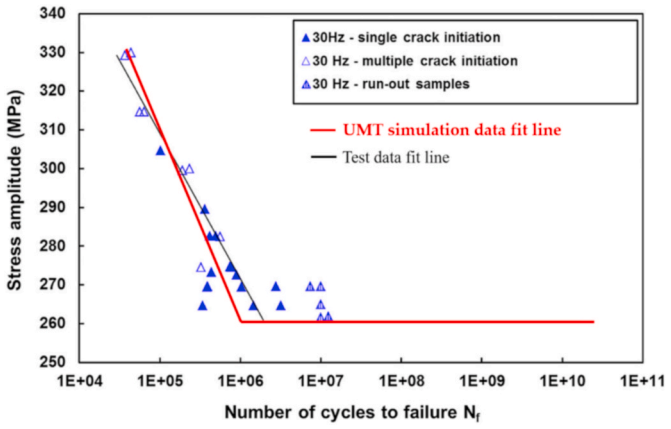

Fig. 17. Comparison of fatigue data and unified mechanics theory predictions for tension-compression fatigue tests on dual phase steel (DP600) without any pre-strain. [The experimental SN curve is obtained from (Torabian et al., 2017)].

of DP600 steel. The thermodynamic fundamental equation of metals under high cycle fatigue is derived. In the simulation, no empirical curve fitting function is needed for fatigue life prediction. The entropy generation due to atomic vacancy configuration, atomic vibration and mass transport are extremely small compared to entropy generation due to microplasticity. It was also assumed that entropy generation due to grain coarsening during high cycle fatigue is negligible.

The entropy generation due to microplasticity is the most dominant entropy generation mechanism. This mechanism can be visualized as a number of microplastic inclusions at localized defect sites inside an elastic matrix which has its own micro-stress, micro-strain based on laws of localization and homogenization. Energy is dissipated through the micro-plastic work at the locations of these inclusions. The number of inclusions increase as TSI ϕ increases from 0 to ϕ_{cr}. Metal high cycle fatigue life prediction results based on the theory of unified mechanics are compared with experimental test data. It is shown that the prediction and test data match very well.

We should emphasize that micro-plastic strain has been used before as a variable to establish an empirical fatigue life function obtained from test data. However, no such empirical function is needed here.

Category 1

Conception and design of study: H.W. Lee, C. Basaran;
Acquisition of data: H.W. Lee;
Analysis and/or interpretation of data: H.W. Lee, C. Basaran.

Category 2

Drafting the manuscript: H.W. Lee;
Revising the manuscript critically for important intellectual content: H.W. Lee, C. Basaran.

Category 3

Approval of the version of the manuscript to be published (the names of all authors must be listed): H,W. Lee, C. Basaran.

Declaration of competing interest

The authors declare that they have no known competing financial interests or personal relationships that could have appeared to influence the work reported in this paper.

Acknowledgements

All persons who have made substantial contributions to the work reported in the manuscript (e.g., technical help, writing and editing assistance, general support), but who do not meet the criteria for authorship, are named in the Acknowledgements and have given us their written permission to be named. If we have not included an Acknowledgements, then that indicates that we have not received substantial contributions from non-authors.

References

Abbaschian, R., Reed-Hill, R.E., 2009. Physical Metallurgy Principles, ISBN 9780495438519.
Atkins, P., Paula, J., et al., 2018. Physical Chemistry, eleventh ed., ISBN 9780198769866.
Basaran, C., 2021. Introduction to Unified Mechanics Theory with Applications. Springer-Nature, ISBN 978-3-030-57772-8.
Basaran, C., Chandaroy, R., 2000. Using finite element analysis for simulation of reliability tests on solder joints in microelectronic packaging. Comput. Struct. 74 (Issue 2), 215–231. https://doi.org/10.1016/S0045-7949(99)00028-0. ISSN 0045-7949.
Basaran, C., Lin, M., 2007a. Electromigration induced strain field simulations for nanoelectronics lead-free solder joints. Int. J. Solid Struct. 44 (14–15), 4909–4924.
Basaran, Cemal, Lin, Minghui, 2007b. Damage mechanics of electromigration in microelectronics copper interconnects. Int. J. Mater. Struct. Integr. 1 https://doi.org/10.1504/IJMSI.2007.013864.
Basaran, C., Lin, Minghui, 2008. Damage mechanics of electromigration induced failure. Mech. Mater. 40 (Issues 1–2), 66–79. https://doi.org/10.1016/j.mechmat.2007.06.006. ISSN 0167-6636.
Basaran, C., Nie, S., 2004. An irreversible thermodynamics theory for damage mechanics of solids. Int. J. Damage Mech. 13 (3), 205–223. https://doi.org/10.1177/1056789504041058.
Basaran, C., Yan, C.Y., 1998. A thermodynamic framework for damage mechanics of solder joints. J. Electron. Packag. Trans. ASME 120, 379–384.
Basaran, C., Zhao, Y., Tang, H., Gomez, J., July 23, 2004. A damage-mechanics-based constitutive model for solder joints. ASME. J. Electron. Packag. September 2005 127 (3), 208–214. https://doi.org/10.1115/1.1939822.
Basaran, Cemal, Lin, Minghui, Ye, Hua, 2004b. A thermodynamic model for electrical current induced damage. In: Proceedings - Electronic Components and Technology Conference, vol. 2, pp. 1738–1745. https://doi.org/10.1109/ECTC.2004.1320353.
Basaran, Cemal, Li, Shidong, Mohd, Fazly, 2008. Thermomigration induced degradation in solder alloys. J. Appl. Phys. 103 https://doi.org/10.1063/1.2943261, 123520 - 123520.
Basaran, Cemal, Li, Shidong, Hopkins, D.C., Veychard, Damien, 2009. Electromigration time to failure of SnAgCuNi solder joints. J. Appl. Phys. 106 https://doi.org/10.1063/1.3159012, 013707 - 013707.
Boltzmann, L., 1877. Über die Beziehung zwischen dem zweiten Hauptsatze des mechanischen Wärmetheorie und der Wahrscheinlichkeitsrechnung, respective den Satzen uber das Wärmegleichgewicht [On the relation between the second law of the mechanical theory of heat and the probability calculus with respect to theorems of thermal equilibrium]. Wiener Berichte II 76, 373–435.
E A Brandes and G B Brook, Smithells Metals Reference Book, seventh ed. seventh ed., ISBN-13: 978-0750636247.
Burton, J.J., 1972. Vacancy-formation entropy in cubic metals. Phys. Rev. B 5 (1972), 2948.
Callen, H.B., 1985. Thermodynamics and Introduction to Thermostatics. John Wiley & Sons, New York.
Callister, W.D., Rethwisch, D.G., 2018. Materials Science and Engineering- an Introduction, tenth ed., ISBN 9781119405498.
Chamati, H., Papanicolaou, N.I., Mishin, Y., Papaconstantopoulos, D.A., 2006. Embedded-atom potential for Fe and its application to self-diffusion on Fe(100). Surf. Sci. 600 (9), 1793–1803. https://doi.org/10.1016/j.susc.2006.02.010.
Charkaluk, Eric, Constantinescu, Andrei, 2009. Dissipative aspects in high cycle fatigue. Mech. Mater. 41 (Issue 5), 483–494. ISSN 0167-6636.
Chu, Y., Gautreau, P., Ragab, T., Basaran, C., 2015. Temperature dependence of Joule heating in Zigzag graphene nanoribbon. Carbon 89, 169–175.
Clausius, R., 1850. Ueber die bewegende kraft Der Wärme und die Gesetze, Welche Sich Daraus Für die Wärmelehre Selbst Ableiten Lassen. Ann. Phys. 79 (4), 368–397, 500–524.
Cugy, P., Galtier, A., 2002. Microplasticity and temperature increase in low carbon steels. In: Blom, A.F. (Ed.), Proc. 8th Int. Fatigue Congress – 3–7 June 2002. EMAS, Barnsley, pp. 549–556.
Doudard, Cédric, Calloch, Sylvain, Cugy, Philippe, Galtier, André, Hild, François, 2005. A probabilistic two-scale model for high-cycle fatigue life predictions. Fatig. Fract. Eng. Mater. Struct. 28 https://doi.org/10.1111/j.1460-2695.2005.00854.x.
Edwards, T., Di Gioacchino, F., Clegg, W., 2021. High resolution digital image correlation mapping of strain localization upon room and high temperature, high cycle fatigue of a TiAl intermetallic alloy. Int. J. Fatig. 142, 105905 https://doi.org/10.1016/j.ijfatigue.2020.105905.
Egner, Władysław, Sulich, Piotr, Mroziński, Stanisław, Egner, Halina, December 2020. Modeling thermo-mechanical cyclic behavior of P91 steel. Int. J. Plast. 135, 102820 https://doi.org/10.1016/j.ijplas.2020.102820.
Fan, Junling, Zhao, Yanguang, Guo, Xinglin, 2018. A unifying energy approach for high cycle fatigue behavior evaluation. Mech. Mater. 120, 15–25. ISSN 0167-6636.
Fultz, B., 2010. Vibrational thermodynamics of materials. Prog. Mater. Sci. 55 (2010), 247–352.
Gao, Shiwu, 1876. Quantum kinetic theory of vibrational heating and bond breaking by hot electrons. Phys. Rev. B 55. https://doi.org/10.1103/PhysRevB.55.1876.
Hajshirmohammadi, B., Khonsari, M.M., 2020. On the entropy of fatigue crack propagation. Int. J. Fatig. 133, 105413 https://doi.org/10.1016/j.ijfatigue.2019.105413. ISSN 0142-1123.
Ho, H.S., Risbet, M., Feaugas, X., 2017. A cyclic slip irreversibility based model for fatigue crack initiation of nickel base alloys. Int. J. Fatig. 102, 1–8. https://doi.org/10.1016/j.ijfatigue.2017.04.007. ISSN 0142-1123.
Imanian, Anahita, Modarres, Mohammad, 2015. A thermodynamic entropy approach to reliability assessment with applications to corrosion fatigue. Entropy 17, 6995–7020.
Jirandehi, A., Khonsari, M., 2021. On the determination of cyclic plastic strain energy with the provision for microplasticity. Int. J. Fatig. 142, 105966 https://doi.org/10.1016/j.ijfatigue.2020.105966.
Kelly, A., Groves, G.W., Kidd, P., 2012. Crystallography and Crystal Defects, ISBN 9780470750148.
Kröner, E., 1961. Zur plastichen verformung des vielkristalls. Acta Metall. 99, 155–161.
Laughlin, D., Hono, K., 2014. Physical Metallurgy, fifth ed., ISBN 9780444537713.
Lemaitre, J., Sermage, J., Desmorat, R., 1999. A two scale damage concept applied to fatigue. Int. J. Fract. 97, 67. https://doi.org/10.1023/A:1018641414428.
Li, Shidong, Mohd, F., Basaran, Cemal, 2008a. Simulating damage mechanics of electromigration and thermomigration. Simulation 84, 391–401. https://doi.org/10.1177/0037549708094856.
Li, Shidong, Mohd, Fazly, Basaran, Cemal, 2008b. Simulating damage mechanics of electromigration and thermomigration. Simulation 84, 391–401. https://doi.org/10.1177/0037549708094856.
Li, S., Abdulhamid, M.F., Basaran, C., 2009. Damage mechanics of low temperature electromigration and thermomigration. IEEE Trans. Adv. Packag. 32 (2), 478–485.
Mankarathodi, Noushad, Kumar, Aman, Rao, Lakshmana, Chebolu, Basaran, Cemal, 2020. Low cycle fatigue life prediction using unified mechanics theory in Ti-6Al-4V alloys. Entropy 22, 24. https://doi.org/10.3390/e22010024.
Marti, Nicolas, Favier, Veronique, Gregori, Fabienne, Saintier, Nicolas, 2020. Correlation of the low and high frequency fatigue responses of pure polycrystalline copper with mechanisms of slip band formation. Mater. Sci. Eng., A 772, 138619. https://doi.org/10.1016/j.msea.2019.138619. ISSN 0921-5093.
Mehdizadeh, M., Ali, Haghshenas, Khonsari, M.M., 2021. On the effect of internal friction on torsional and axial cyclic loading. Int. J. Fatig. 145, 106113 https://doi.org/10.1016/j.ijfatigue.2020.106113. ISSN 0142-1123.
Mishin, Yuri, S⊘rensen, Mads R., Voter, Arthur F., 2001. Calculation of point-defect entropy in metals. Philos. Mag. A 81 (11), 2591–2612. https://doi.org/10.1080/01418610108216657.
Mozafari, F., Thamburaja, P., Srinivasa, A., Abdullah, S., 2020. Fatigue life prediction under variable amplitude loading using a microplasticity-based constitutive model. Int. J. Fatig. 134, 105477 https://doi.org/10.1016/j.ijfatigue.2020.105477.
Mughrabi, H., 2009. Cyclic slip irreversibilities and the evolution of fatigue damage. Metall. Mater. Trans. 40, 1257–1279. https://doi.org/10.1007/s11661-009-9839-8.
Mughrabi, Hael, 2013. Cyclic slip irreversibility and fatigue life: a microstructure-based analysis. Acta Mater. 61 (4), 1197–1203. https://doi.org/10.1016/j.actamat.2012.10.029. ISSN 1359-6454.
Naderi, M., Amiri, M., Khonsari, M.M., 2010. On the thermodynamic entropy of fatigue fracture. Proc. Royal. Soc. A 466. https://doi.org/10.1098/rspa.2009.0348.
Osara, Jude A., Bryant, Michael D., 2019. Thermodynamics of fatigue: degradation-entropy generation methodology for system and process characterization and failure analysis. Entropy 21 (7), 685. https://doi.org/10.3390/e21070685.
Planck, M., 1900. Section 134: entropie und Warscheinlichkeit. In: Vorlesungen uber die theorie der wurmestrahlung. J.A. Barth, Leipzig, Germany.
Plimpton, S., 1995. Fast parallel algorithms for short-range molecular dynamics. J. Comput. Phys. 117, 1–19.
Ragab, T., Basaran, C., 2009. " Joule heating in single-walled carbon nanotubes. J. Appl. Phys. 106, 063705.
Ribeiro, Patrick, Petit, Johann, Gallimard, Laurent, July 2020. Experimental determination of entropy and exergy in low cycle fatigue. Int. J. Fatig. 136, 105333.
Temfack, T., Basaran, C., 2015. Experimental verification of thermodynamic fatigue life prediction model using entropy as damage metric. Mater. Sci. Technol. 31 (13), 1627–1632. https://doi.org/10.1179/1743284715Y.0000000074.
Teng, Z., Wu, H., Boller, C., Starke, P., 2020a. A unified fatigue life calculation based on intrinsic thermal dissipation and microplasticity evolution. Int. J. Fatig. 131, 105370 https://doi.org/10.1016/j.ijfatigue.2019.105370.
Teng, Zhenjie, Wu, Haoran, Boller, Christian, Peter, Starke, 2020b. Thermodynamic entropy as a marker of high-cycle fatigue damage accumulation: example for normalized SAE 1045 steel. Fatig. Fract. Eng. Mater. Struct. 1–13.
Teng, Zhenjie, Wu, Haoran, Boller, Christian, Starke, Peter, 2020c. Thermodynamic entropy as a marker of high-cycle fatigue damage accumulation: example for normalized SAE 1045 steel. Fatig. Fract. Eng. Mater. Struct. 43 https://doi.org/10.1111/ffe.13303.
Thomson, W., 1853. On the dynamical theory of heat, with numerical results deduced from Mr Joule's equivalent of a thermal unit, and M. Regnault's observations on steam. Trans. R. Soc. Edinb. 20 (2), 261–288. https://doi.org/10.1017/S0080456800033172.

Torabian, Noushin, Favier, Véronique, Dirrenberger, Justin, Adamski, Frédéric, Ziaei-Rad, Saeed, Ranc, Nicolas, 2017. Correlation of the high and very high cycle fatigue response of ferrite based steels with strain rate-temperature conditions. Acta Mater. 134, 40–52. https://doi.org/10.1016/j.actamat.2017.05.064. ISSN 1359-6454.

Ustrzycka, A., Mróz, Z., Kowalewski, Z., Kucharski, S., 2020. Analysis of fatigue crack initiation in cyclic microplasticity regime. Int. J. Fatig. 131, 105342 https://doi.org/10.1016/j.ijfatigue.2019.105342.

Wang, Jundong, Yao, Yao, 2017. An entropy based low-cycle fatigue life prediction model for solder materials. Entropy 19, 503.

Wang, Jundong, Yao, Yao, 2019. An entropy-based failure prediction model for the creep and fatigue of metallic materials. Entropy 21 (11), 1104. https://doi.org/10.3390/e21111104.

Wollenberger, H.J., 1996. Physical Metallurgy, fourth ed., ISBN 9780444898753.

Xue, H.Q., Bayraktar, E., Bathias, C., 2008. Damage mechanism of a nodular cast iron under the very high cycle fatigue regime. J. Mater. Process. Technol. 202 (Issues 1–3), 216–223. ISSN 0924-0136.

Yao, W., Basaran, C., 2012. Electromigration analysis of solder joints under ac load: a mean time to failure model. J. Appl. Phys. 111 (6), 063703.

Yao, Wei, Basaran, Cemal, 2013a. Electromigration damage mechanics of lead-free solder joints under pulsed DC: a computational model. Comput. Mater. Sci. 71, 76–88. https://doi.org/10.1016/j.commatsci.2013.01.016.

Yao, W., Basaran, C., 2013b. Computational damage mechanics of electromigration and thermomigration. J. Appl. Phys. 114, 103708.

Yao, Wei, Basaran, Cemal, 2013c. Damage mechanics of electromigration and thermomigration in lead-free solder alloys under alternating current: an experimental study. Int. J. Damage Mech. 23, 203–221. https://doi.org/10.1177/1056789513488396.

Ye, H., Basaran, C., Hopkins, D.C., 2004. Deformation of solder joint under current stressing and numerical simulation—I. Int. J. Solid Struct. 41 (18–19), 4939–4958.

Ye, H., Basaran, C., Hopkins, D.C., 2006. Experimental damage mechanics of micro/power electronics solder joints under electric current stresses. Int. J. Damage Mech. 15 (1), 41–67.

Young, Colin, Subbarayan, Ganesh, 2019. Maximum entropy models for fatigue damage in metals with application to low-cycle fatigue of aluminum 2024-T351. Entropy 21 (10), 967. https://doi.org/10.3390/e21100967.

Yun, Huisung, Modarres, Mohammad, 2019a. Measures of entropy to characterize fatigue damage in metallic materials. Entropy 21 (8), 804. https://doi.org/10.3390/e21080804.

Yun, Huisung, Modarres, Mohammad, 2019b. Measures of entropy to characterize fatigue damage in metallic materials. Entropy 2019 21 (8), 804.